JACS
JOURNAL OF THE AMERICAN CHEMICAL SOCIETY
Article
pubs.acs.org/JACS

Nucleation of NaCl from Aqueous Solution: Critical Sizes, Ion-Attachment Kinetics, and Rates

Nils E. R. Zimmermann,[†,∥] Bart Vorselaars,[§,⊥] David Quigley,[§] and Baron Peters*[,†,‡]

[†]Department of Chemical Engineering and [‡]Department of Chemistry and Biochemistry, University of California, Santa Barbara, California 93106, United States

[§]Department of Physics and Centre for Scientific Computing, University of Warwick, Coventry, CV4 7AL, U.K.

Supporting Information

ABSTRACT: Nucleation and crystal growth are important in material synthesis, climate modeling, biomineralization, and pharmaceutical formulation. Despite tremendous efforts, the mechanisms and kinetics of nucleation remain elusive to both theory and experiment. Here we investigate sodium chloride (NaCl) nucleation from supersaturated brines using seeded atomistic simulations, polymorph-specific order parameters, and elements of classical nucleation theory. We find that NaCl nucleates via the common rock salt structure. Ion desolvation—not diffusion—is identified as the limiting resistance to attachment. Two different analyses give approximately consistent attachment kinetics: diffusion along the nucleus size coordinate and reaction-diffusion analysis of approach-to-coexistence simulation data from Aragones et al. (J. Chem. Phys. 2012, 136, 244508). Our simulations were performed at realistic supersaturations to enable the first direct comparison to experimental nucleation rates for this system. The computed and measured rates converge to a common upper limit at extremely high supersaturation. However, our rate predictions are between 15 and 30 orders of magnitude too fast. We comment on possible origins of the large discrepancy.

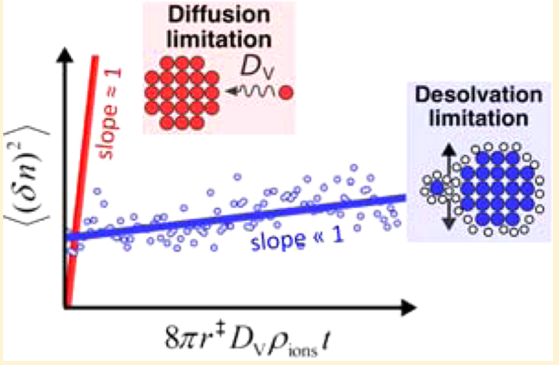

INTRODUCTION

The kinetics of nucleation poses notorious challenges to theory,[1] to simulations,[2] and even to experiments.[3] Accurate predictions and experiments remain challenging for all types of phase transitions: freezing of supercooled liquids,[4,5] condensation of supercooled vapors,[6,7] nucleate boiling of superheated liquids,[8,9] homogeneous melting of superheated solids,[10,11] solid−solid polymorph transitions,[12,13] polymer crystallization,[14] and magnetic domain reversal.[15] Even seemingly simple transitions, like the freezing of water, continue to yield surprises.[16−20] In the absence of potent nucleants,[21,22] seeds,[23] and nucleation templates,[24,25] a free energy barrier impedes the transition from a metastable phase to a more stable phase. The slow nucleation kinetics manifests as observable induction times[26−29] and metastable zones[30−33] in the phase diagram.

Once the first nucleus forms from perhaps tens of atoms, the new stable phase can grow irreversibly to macroscopic size. The first nucleation events are especially important because subsequent growth of postcritical nuclei changes the thermodynamic conditions in the surrounding environment. Typical experiments probe large systems, for which it is difficult to eliminate all impurities; therefore, the species and/or sites responsible for nucleation are unclear. Simulations can omit the problem of impurities and interfaces to focus on idealized homogeneous nucleation processes. They probe, however, extremely small volumes and short time scales, rendering the observation of a nucleation event almost impossible without specialized rare-events methods. Seeding approaches in closed simulations[34] can circumvent the time-scale problem if the nucleus growth velocity, $\mathrm{d}\langle n\rangle/\mathrm{d}t$, fulfills the following criterion:

$$\Delta t \frac{\mathrm{d}\langle n\rangle}{\mathrm{d}t} \ll c_{\mathrm{sat}} V (S-1) \tag{1}$$

where n is the nucleus size, t the time, Δt the duration of the seeded trajectory, S the supersaturation (c/c_{sat}), c_{sat} the solute concentration at saturation, and V the volume of the initial solution. Inequality 1 ensures that the supersaturation is not depleted during the short trajectories that are used to quantify drift and diffusion along the nucleus size axis.[34] For simulations in which nuclei are grown from solution (i.e., not from seeds), the simulation box should be large enough to satisfy

$$n^{\ddagger} \ll c_{\mathrm{sat}} V (S-1) \tag{2}$$

where $n^{\ddagger}$ is the critical nucleus size. Inequalities 1 and 2 emerge from analyses of depletion effects that occur as a solute nucleus removes solute from a tiny volume of supersaturated solution.[35] Peters and co-workers noted[2,36,37] that early simulations of solute precipitate nucleation were using closed *NVT* simulations without ensuring that inequalities 1 and/or 2 were satisfied.

Received: August 1, 2015
Published: September 15, 2015

DOI: 10.1021/jacs.5b08098
J. Am. Chem. Soc. 2015, 137, 13352−13361

Theoretically, nucleation rates are extremely sensitive to supersaturation. Therefore, finite size effects, which modify the supersaturation during simulations of the nucleation process, are likely to cause errors in predicted rates and mechanisms.

Grand-canonical simulations[38,39] could in principle eliminate finite size effects by imposing a constant chemical potential of ions in the solution phase. However, low acceptance rates[40] render such approaches computationally infeasible. Furthermore, insertions of ions near the growing nucleus[41] or insertions of fractional particles[42] may lead to unphysical effects, which may ultimately obscure the true nucleation mechanisms and rates. Perego et al.[43] recently developed a constant chemical-potential molecular dynamics (MD) algorithm. The method requires simulation of a solute reservoir, transition regions, and a region of constant chemical potential, μ. Such approaches may prove useful in future studies. At present, the most practical approaches are NpT simulations with finite-size corrections[2,35,37,44−47] or uncorrected simulations that obey inequality 1 or 2.

Sodium chloride precipitation from aqueous solution offers an attractive model system for predicting nucleation rates from simulations for two reasons. First, there are atomistic force fields[48] that accurately predict key properties: solution chemical potentials,[49] solubility limits,[48,49] and diffusivities of NaCl in water.[48] Second, a few measurements are available for this system. Importantly, the experimental studies attempted to observe homogeneous NaCl nucleation by working with small volumes and controlled interfaces.

Na et al.[26] levitated aqueous NaCl droplets while evacuating water vapor from the surrounding atmosphere to gradually increase the supersaturation. Eventually, NaCl crystals formed in the droplet, allowing them to determine the induction time, t_{ind}. By using classical nucleation theory (CNT), they estimated the interfacial free energy, γ, between the supersaturated brine and rock salt as 87 mJ/m^2. The typical supersaturation at the moment of crystallization was $S = m/m_{sat} = 2.31$, where m denotes the NaCl formula unit molality in solution. Olsen et al.[27] reassessed the typical NaCl nucleation rate with an automated version of the levitation technique so that they could probe longer induction times ($t_{ind} > 1$ h). Gao et al.[28] measured efflorescence relative humidities of airborne NaCl−$NaSO_4$ particles of varying composition with a tandem differential mobility analyzer coupled with an exposure chamber. Nucleation rates were approximated on the basis of CNT and mean residence times in the efflorescence chamber (instead of induction times). Desarnaud et al.[29] investigated NaCl nucleation and growth in micro-capillaries of different sizes, shapes, and surface chemistries. They slowly evaporated water from initially undersaturated NaCl solutions confined by the capillaries. Their microscopy images revealed that crystals formed far away from any surfaces and interfaces. Furthermore, rate predictions based on CNT and literature data agreed well with their induction times, for which reason they concluded that homogeneous nucleation had occurred. Rates estimated from the data of Gao et al.,[28] Na et al.,[26] Olsen et al.,[27] and Desarnaud et al.[29] are approximately 10^{13}/cm^3/s, 10^9/cm^3/s, 10^4/cm^3/s, and 10^{-9}/cm^3/s, respectively. Details on these experiment-based rate estimates can be found in the Supporting Information. Importantly, the rates were measured at three different supersaturations and using three very different methods. There are currently no measured rates of NaCl nucleation from aqueous solution that span wide and overlapping supersaturation intervals.

Nucleation of NaCl from aqueous solution has been simulated in several earlier works.[50−55] Zahn,[50] Alejandre and Hansen,[55] as well as Giberti et al.[51] used transition path sampling and metadynamics with closed NVT trajectories and no tests of inequality 1 or 2. Zahn[50] observed that ion aggregates were particularly stable when an Na^+ ion was octahedrally coordinated by Cl^- ions. The study by Alejandre and Hansen[55] found that the nucleation mechanism is extraordinarily sensitive to small changes in the force field. Giberti et al.[51] employed metadynamics simulations to find an intriguing wurtzite-like polymorph, which was suggested to be an intermediate en route from brine to the final rock salt structure. Chakraborty and Patey[52,53] performed direct large-scale simulations of nucleation and growth. Their approach seems to have satisfied inequality 2 because the critical nuclei were small, the brine reservoir was large, and the supersaturation was high (albeit not precisely known). Rock salt nucleated via a two-step mechanism: first, a dense but unstructured NaCl nucleus formed, which, in the second step, rearranged into the rock salt structure. Such two-step nucleation mechanisms[56−60] are easily rationalized (1) when the amorphous phase has greater stability than the metastable solution,[61] so that amorphous particles grow to macroscopic sizes, and (2) when there is a metastable fluid−fluid critical point within the miscibility gap of the solid and the dilute solution.[56] Neither of these explanations applies to NaCl−water mixtures, but potentially other factors could drive a two-step nucleation mechanism.[2,62] On the simulation front, there is a need for studies of solute precipitate nucleation rates and mechanisms that systematically consider the effects of supersaturation and/or temperature.

In this work, we compute NaCl nucleation rates and investigate the attachment kinetics at three supersaturations using atomistic simulations. We use the best currently available force fields,[48] for which Aragones et al.[49] provided an accurate chemical potential driving force. We develop two local order parameters that can mutually distinguish ions located in supersaturated solution, rock salt-like, and wurtzite-like crystalline environments. The order parameters are used to monitor the evolution of nucleus size in ensembles of trajectories where crystalline seeds are merged with supersaturated solutions. Following the method of Knott et al.,[34] mean drift velocity and diffusive spreading rates along the nucleus size coordinate are then used to determine the interfacial free energy and the attachment frequency. Subsequently, we estimate the free energy barrier to nucleation, the prefactor, and finally the rate of NaCl nucleation from aqueous solution at three supersaturations, which bracket the conditions of the aforementioned experiments.

FORCE FIELD AND SUPERSATURATION

According to classical nucleation theory, the free energy to form a nucleus of n atoms is[2,3]

$$F(n) = -n\Delta\mu + \gamma a n^{2/3} \tag{3}$$

The first term arises from the thermodynamic driving force, which favors formation of the new phase. The second term reflects the cost of creating an interfacial area between the evolving nucleus and the surrounding solution. Initially, the interfacial term increases rapidly with nucleus size, but at later stages, the bulk driving force term dominates. The two contributions balance at the critical size $n^‡$, where $\partial F/\partial n = 0$. Predictions based on CNT usually employ the interfacial free energy of a flat macroscopic interface and the macroscopic chemical potential difference between the *bulk* metastable and stable phases ($\Delta\mu$) and assume spherical shapes. Many sources of

DOI: 10.1021/jacs.5b08098
J. Am. Chem. Soc. 2015, 137, 13352−13361

error have been noted in the CNT framework. For example, there cannot be a sharp division between stable and metastable phases at the nanoscale. Second, the macroscopic interfacial free energy is not appropriate for the nanoscale. Nevertheless, many studies suggest that approximate agreement with classical nucleation theory can be obtained with a modified interfacial free energy.[63−66]

CNT predicts a strong and specific dependence on supersaturation that is often confirmed in experiments. Hence, predicted and measured rates should be compared at corresponding supersaturations. The importance of supersaturation for nucleation makes solubility the most important property for choosing an appropriate model. Several force fields are available for water,[67−69] for Na^+ and Cl^- ions,[70] and for their mixtures.[48,71−73] Joung and Cheatham[48] developed force field parameters of Na^+ and Cl^- ions that give approximately correct solubilities when used with SPC/E water. Aragones et al.[49] performed an in-depth reassessment[74] of the NaCl solubility in SPC/E water for three common NaCl force fields: Tosi−Fumi,[70,71] Smith−Dang,[72] and Joung−Cheatham.[48] This work uses the Joung−Cheatham model, which gave the solubility (m = 5.1 mol_{NaCl}/kg_{H2O}) closest to the experimental value (6.15).[49] Furthermore, Aragones et al.[49] provided a functional relationship between the chemical potential of sodium chloride in solution and NaCl molality for the Joung−Cheatham model. Their results provide a precise concentration-dependent driving force for nucleation in terms of NaCl formula units:

$$\Delta\mu_{NaCl}(m) = \mu_{NaCl}(m) - \mu_{NaCl}(m_{sat}) \quad (4)$$

The Joung−Cheatham parameters for Na^+ and Cl^- ions as well as the SPC/E water parameters are provided in the Supporting Information (section SI1.1). The short-range cutoff for the Lennard-Jones interactions was 9 Å, and tail corrections were implemented as described by Aragones et al.[49] A particle−particle particle−mesh algorithm[75] treated the long-range electrostatic part of the potential. SHAKE[76] retained the geometry of rigid water molecules. LAMMPS[77] was used to integrate Nosé−Hoover-style equations of motion,[78] in which target temperature and pressure were T = 298 K and p = 1 bar.

We reproduced the total number density, ρ_N, as a function of molality reported by Aragones et al.[49] to verify our simulation procedure (Figure 1a). After 0.5 ns equilibration, the average box volume of each NpT simulation was calculated over a time of another 0.5 ns. Three independent simulations were performed for each molality and box size to obtain simulation box size averages. Our simulation results are indistinguishable from those of Aragones et al.[49] Because we perform simulations of nucleation at higher NaCl concentrations than those reported by Aragones et al.,[49] we extended their results from m = 8 to 12 mol_{NaCl}/kg_{H2O}. This required a third-order polynomial (blue curve in Figure 1a) instead of the second-order polynomial[49] (gray curve) to accurately describe the density at high molalities with an analytical expression.

The new density relationship was subsequently incorporated into the ideal term of the Helmholtz free energy that contributed to the NaCl solution chemical potential expression $\mu_{NaCl}(m)$ (Figure 1b). This enabled estimation of the driving force at higher molalities. The residual part of the free energy contributing to the chemical potential was not changed. In this context, Figure 1 indicates that the uncertainty in driving force at high molalities seems small: roughly 10% based on the maximal deviation between modified μ-expression from this work and the original one by Aragones et al.[49]

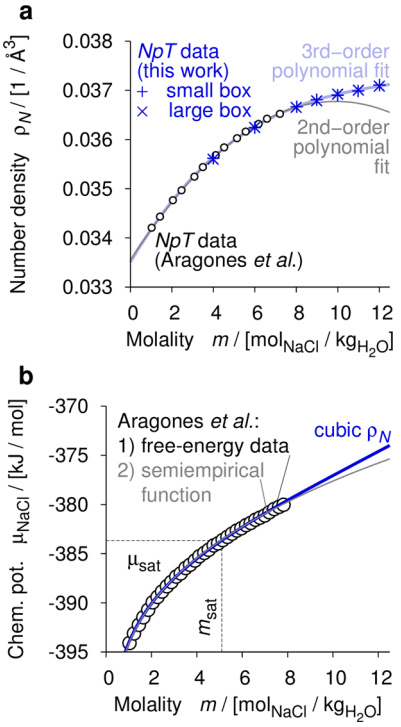

Figure 1. (a) Total number density, ρ_N, and (b) chemical potential of sodium chloride, μ_{NaCl}, as functions of molality, m, for under- and supersaturated aqueous NaCl solutions (T = 298 K, p = 1 bar). We have extended the density relationship provided by Aragones et al.[49] (gray line) to also capture the high-molality region (blue line) and incorporated it into the chemical potential expression. Both expressions are found in the Supporting Information (section SI1.1).

POLYMORPH SPECIFIC NUCLEUS SIZE COORDINATES

Collective variables and order parameters are useful for modeling the dynamics of processes where the reaction coordinates are not specific bond lengths and angles. Theories and simulations of nucleation use structural order parameters to distinguish between crystalline and disordered regions. Giberti et al.[51] reported wurtzite-like NaCl clusters along with the expected rock salt NaCl clusters. Therefore, we developed new order parameters that can mutually distinguish ions in solution, rock salt-like, and wurtzite-like environments. A simple coordination number, $\theta(i)$, counts the number of ions within a predefined distance r_θ from a tagged ion i. At the concentrations probed in this study, most ions in solution (>85%) have just 0, 1, or 2 neighboring ions within a distance r_θ. Ions in crystallites or unstructured aggregates will have more neighboring ions. Distinguishing rock salt and wurtzite-like environments requires further information about the geometry of the neighboring counterions. Ions that are completely embedded in a wurtzite environment have four counterion neighbors arranged in a tetrahedron (Figure 2a). Ions that are completely embedded in a rock salt environment have six counterion neighbors arranged in an octahedron (Figure 2b).

To compute the polymorph-specific coordination numbers, the coordination sphere of a tagged ion is compared to ideal structural templates for the two polymorphs.[79−82] The "distance" between the local environment of the tagged ion and the ideal template is calculated by using internal coordinates based on a rotation-invariant local coordinate system.[80] Specifically, two neighboring counterions are used to construct a spherical polar

DOI: 10.1021/jacs.5b08098
J. Am. Chem. Soc. 2015, 137, 13352−13361

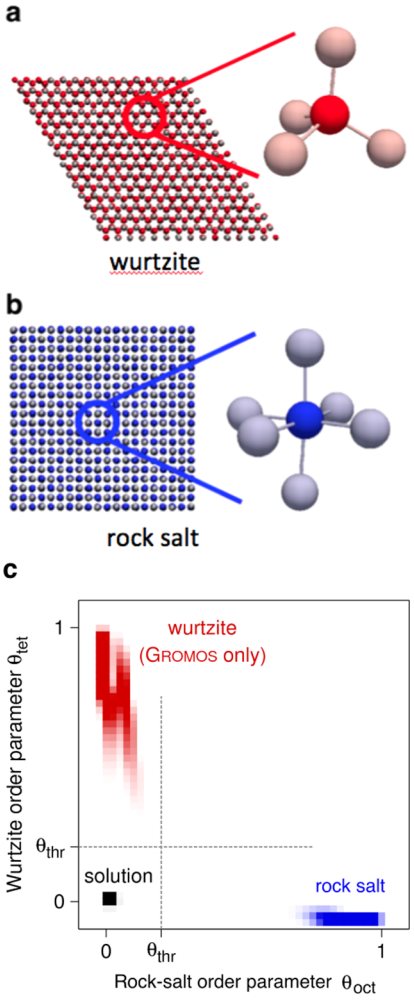

Figure 2. Local environment recognized by (a) the wurtzite-specific order parameter, θ_{tet}, and (b) the rock salt order parameter, θ_{oct}. (c) Joint probability distributions, $P(\theta_{oct},\theta_{tet})$, from simulations of a bulk rock salt (blue) and a bulk NaCl-wurtzite crystal structure (red) as well as from a supersaturated solution (m = 8); the white color corresponds to P = 0. The polymorph-specific order parameters θ_{tet} and θ_{oct} can distinguish between all three phases if they are used together with a single threshold of θ_{thr} = 0.2.

coordinate system around the tagged ion and to predict where additional atoms in the coordination sphere would be if the coordination sphere was perfect. The polymorph-specific coordination number is a sum of Gaussians that decay with deviations between positions of actual ions in the coordination sphere from their ideal positions. The influence of distance between adjacent ions is accounted for by the a priori chosen cutoff distance, r_θ, only. Both coordination numbers are normalized so that they take the value of 1 when the environment around the tagged ion exactly matches the reference crystal structure. A tagged atom i is identified as rock salt-like if the coordination order parameter exceeds a threshold (i.e., $\theta_{oct}(i) > \theta_{thr}$); similarly, if $\theta_{tet}(i) > \theta_{thr}$ then atom i is in a tetrahedral wurtzite-like environment. The functional forms of the order parameters can be found in the Supporting Information (section SI1.2). Note that a tagged ion i must have at least four counterion neighbors to be classified as tetrahedral or rock salt-like.

Both r_θ and θ_{thr} were carefully optimized for the rock salt order parameter using likelihood maximization and overlap minimization procedures[83,84] to obtain r_θ = 4.1 Å and θ_{thr} = 0.43. We found that the GROMOS force field[85] exaggerates the stability of the wurtzite phase. The Joung−Cheatham model,[48] on the other hand, captures the relative stability of the two polymorphs with remarkable accuracy (see section SI1.5 of the Supporting Information for further information). Because it was specifically developed for simulations near the NaCl solubility limit, the Joung−Cheatham model[48] is the preferred model for crystallization studies. For these reasons, we will not consider the NaCl-wurtzite polymorph or further optimize the wurtzite nucleus size coordinate in this work.

To monitor the progress of nucleation, we determined the largest contiguous cluster, n, of ions that fulfilled three criteria.[86] First, the cluster can only contain ions whose rock-salt order parameter exceeds the threshold value, θ_{thr}. Second, the rock salt-like ions must not be separated by a distance longer than r_θ. Third, adjacent rock salt-like ions must be of opposite type (Na^+ vs Cl^-). A clustering algorithm using these rules provides the cluster size n with no assumptions about nucleus shape. Note that we cluster ions rather than formula units. Therefore, we define the chemical potential driving force as

$$\Delta\mu = 0.5\Delta\mu_{NaCl} \quad (5)$$

to ensure compatibility between eqs 3 and 4. Equation 5 reflects the assumption that Na^+ and Cl^- ions in the nucleus contribute equally to its chemical potential, regardless of the actual composition.

CRITICAL NUCLEUS SIZE

In order to calculate the nucleation rate, we followed a seeding strategy.[34] Compact electroneutral nuclei were cut from a bulk rock-salt structure and placed into supersaturated solutions (Figure 3). We discarded overlapping solution molecules with the constraint of preserving the electroneutrality of the resulting merged configuration. A three-stage equilibration procedure was used to anneal the interfaces of the seeds (for details, see section SI1.3 of the Supporting Information). Box volumes were chosen such that distances between periodic images of the cluster ions always exceeded the interaction cutoff radius and also the (much shorter) Debye length.[87]

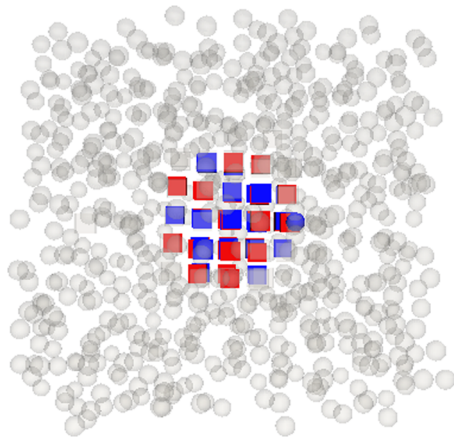

Figure 3. Largest contiguous cluster of sodium (red) and chloride ions (blue) from merging a seed configuration cut from a bulk rock salt structure with a configuration of a supersaturated solution (m = 12). Water molecules are omitted for clarity. Ions that do not belong to the largest cluster are gray. Cubes represent ions that originally came from the seed, whereas ions that were initially part of the solution configuration are displayed as spheres.

DOI: 10.1021/jacs.5b08098
J. Am. Chem. Soc. 2015, 137, 13352−13361

After the equilibration steps, the nuclei are allowed to freely evolve as swarms of trajectories. Swarms are initiated from a series of different sizes, and the trajectories in each swarm are allowed to evolve in time for 10 ns. Each swarm contains five independent trajectories, and Figure 4 shows the average

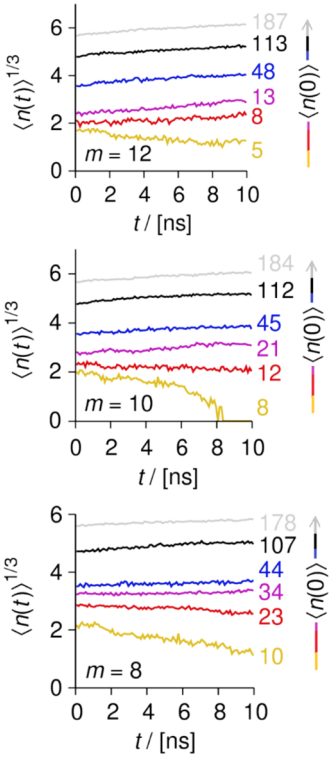

Figure 4. Cubic root of nucleus size that was averaged over five independent simulations, $\langle n(t)\rangle^{1/3}$, depends linearly on time. Note that the initial sizes, $\langle n(0)\rangle$, were obtained from fitting. Tests of inequality 1 for each of these conditions are given in the Supporting Information (section SI2.1).

behavior $\langle n(t)\rangle$ as a function of time. At each molality (supersaturation), there is a critical size $n^{\ddagger}$ such that $\mathrm{d}\langle n\rangle/\mathrm{d}t \sim 0$ when $n^{\ddagger} = \langle n(0)\rangle$. The critical sizes are $n^{\ddagger} = 31$, 14, and 6 at $m =$ 8, 10, and 12 $\mathrm{mol_{NaCl}/kg_{H2O}}$. Note that $n^{\ddagger}$ decreases with increasing supersaturation, as expected from CNT. Swarms initiated from seeds larger than the critical size tend to grow ($\mathrm{d}\langle n\rangle/\mathrm{d}t > 0$), while swarms initiated from seeds smaller than the critical size tend to shrink ($\mathrm{d}\langle n\rangle/\mathrm{d}t < 0$).

■ ATTACHMENT FREQUENCY

The ion attachment frequency to the critical nucleus was calculated from the time-dependent mean square changes in nucleus size,[34,86] $\langle[\delta n(t)]^2\rangle$, where $\delta n(t) = n(t) - \langle n(t)\rangle$. The term $\langle n(t)\rangle$ is important because it corrects for possible drift in the nucleus size coordinate. The drift and diffusion can be separately examined by computing multiple trajectories from the same initial configuration, that is, by examining swarms of trajectories.[34,88] For each driving force, we computed swarms from 25 configurations with four trajectories per swarm. Thus, in total, we examined 100 trajectories per supersaturation, with each trajectory of duration 500 ps. The four trajectories from each configuration were initiated with different initial ion momenta but with the same momenta for the rigid water molecules, because randomly drawn momenta are incompatible with SHAKE implementations in standard MD packages.[89] Nevertheless, the random velocities on the NaCl ions were sufficient to give rapidly diverging trajectories.

The value of the diffusivity along the nucleus size is typically determined[34,86,90] from the slope of a plot of $\langle(\delta n)^2\rangle$ vs t:

$$D = \mathrm{d}\langle(\delta n)^2\rangle/2\mathrm{d}t \tag{6}$$

We have conducted the same analysis here to determine the attachment frequency, D, at the critical size, which is an important parameter in the nucleation rate. However, the magnitude of D and its nucleus-size dependence[2] provide additional insight on the *mechanism* of ion attachment.

The attachment frequency reflects one or both of two resistances: diffusion through the bulk solution toward the nucleus or an ion-desolvation barrier to incorporation at the surface of the nucleus. The two limiting cases lead to two different expressions[2] for the attachment frequency:

$$D = \begin{cases} 4\pi r^{\ddagger} D_{\mathrm{V}} \rho_{\mathrm{ions}} & \text{bulk diffusion limited} \\ 4\pi (r^{\ddagger})^2 k_{\mathrm{S}} \sigma_{\mathrm{S}} \rho_{\mathrm{ions}} & \text{ion desolvation limited} \end{cases} \tag{7a,7b}$$

Here D_{V} denotes the spatial diffusion coefficient of the NaCl electrolyte, $r^{\ddagger}$ is the radius of the (critical) nucleus, k_{S} is a second-order rate constant with units $\mathrm{m^3/(site\ ion\ s)}$ for ion attachment, σ_{S} is the surface concentration of attachment sites in $\mathrm{site/m^2}$, and ρ_{ions} is the bulk concentration of ions ($=2\rho_{\mathrm{NaCl}}$). Because of eqs 7a,7b, we can interpret the attachment frequency according to the predictions from two possible mechanisms. For diffusion-limited attachment, we should find

$$\frac{\mathrm{d}\langle(\delta n)^2\rangle/\mathrm{d}t}{8\pi r^{\ddagger} D_{\mathrm{V}} \rho_{\mathrm{ions}}} \approx 1 \quad \text{(diffusion limited)} \tag{8}$$

whereas desolvation-limited attachment should yield

$$\frac{\mathrm{d}\langle(\delta n)^2\rangle/\mathrm{d}t}{8\pi r^{\ddagger} D_{\mathrm{V}} \rho_{\mathrm{ions}}} = r^{\ddagger} k_{\mathrm{S}} \sigma_{\mathrm{S}} / D_{\mathrm{V}} \ll 1 \quad \text{(desolvation limited)} \tag{9}$$

In this way, we can identify both the mechanism and, if applicable, the parameter $k_{\mathrm{S}}\sigma_{\mathrm{S}}$ for attachment. As seen from Figure 5, the attachment frequency is $o(100)$ times smaller than expected for diffusion-controlled attachment. Therefore, ion attachment is desolvation-limited.

The results in Figure 5 can be combined with the known electrolyte diffusivity D_{V} and the critical nucleus sizes determined in Figure 4 to provide an estimate of $k_{\mathrm{S}}\sigma_{\mathrm{S}}$. All three driving forces yield similar slopes, suggesting that $k_{\mathrm{S}}\sigma_{\mathrm{S}}$ is only a weak function of nucleus size. Using data from the three molalities together gives a common estimate of $k_{\mathrm{S}}\sigma_{\mathrm{S}} = 0.066$ m/s.

Interestingly, the direct-coexistence simulations that Aragones et al.[49] used to compute the NaCl solubility can be reanalyzed to independently estimate $k_{\mathrm{S}}\sigma_{\mathrm{S}}$. As depicted in Figure 6a, Aragones et al.[49] brought a rock salt slab into contact with a supersaturated solution of molality $m \approx 7.25$ mol/kg. The average molality in the core solution (region iii) dropped toward the saturation value (m = 5.5 mol/kg) on the time scale of 1 μs, as ions attached to the faces of the NaCl slab (region i).

When the electrolyte diffusivity is concentration-independent and electrolyte concentration differences are small, the spatiotemporal electrolyte concentration follows Fick's second law. The initial and final concentrations in the simulations of Aragones et al.[49] are quite similar (only 30% different). Thus, Fick's second law, $\partial\rho/\partial t = D_{\mathrm{V}}\partial^2\rho/\partial z^2$, should be applicable.

DOI: 10.1021/jacs.5b08098
J. Am. Chem. Soc. 2015, 137, 13352−13361

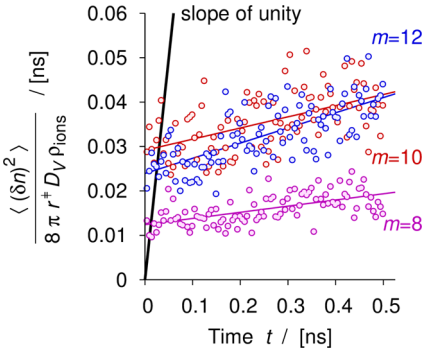

Figure 5. Time evolution of the mean square change in size of critical nuclei, $\langle(\delta n)^2\rangle$, divided by the expected frequency for attachment that is limited by bulk ion diffusion. The slope is much less than unity, indicating that desolvation limitation takes place. Therefore, the slopes correspond to the quantity $r^{\ddagger}k_S\sigma_S/D_V$. The nonzero intercept is commonly observed in nucleation[34,90] and stems from "flickering", that is, from small atom displacements that transiently add and remove atoms from the largest cluster.

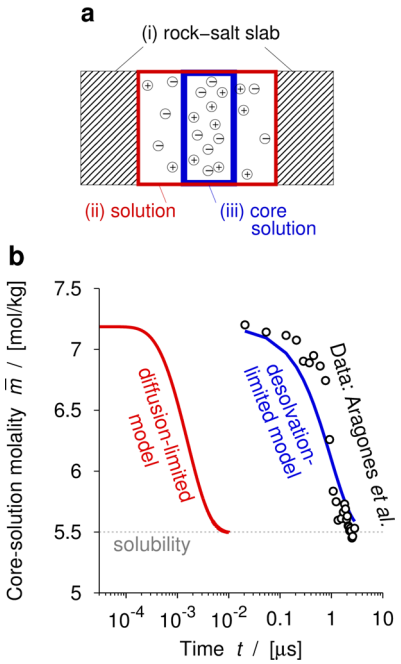

Figure 6. (a) Different regions in direct-coexistence simulations by Aragones et al.[49] (b) The depletion of the NaCl molality in the 20 Å thick core-solution region reported by the authors (circles) cannot be explained by a diffusion-limited attachment model (red curve). Boundary conditions for desolvation-limited attachment kinetics (blue curve) yield much better agreement with their simulation data.

Moreover, we have observed a linear relationship between molality and concentration for the small interval 5.5 mol/kg < m < 7.2 mol/kg, that is, for the range between initial and final molality in the simulations of Aragones et al.[49] Hence, we can directly replace ρ with molality m in the diffusion equation. The same linear relationship between m and ρ allows us to write boundary conditions in terms of molality differences and gradients. The most general "Robin-type" boundary condition accounts for either diffusion-limited or desolvation-limited attachment cases:

$$-D_V \left.\frac{\partial m}{\partial z}\right|_{\pm L} = \frac{1}{2}k_S\sigma_S(m_{\pm L} - m_{sat}) \tag{10}$$

where the factor of $^1/_2$ accounts for the conversion from individual ions to NaCl formula units. The equations can be solved by standard eigenfunction expansion approaches. In terms of $\phi(z,t) = [m(z,t) - m_{sat}]/[m(z,0) - m_{sat}]$ the solution is

$$\phi(z,t) = \sum_{i=1}^{\infty} A_i e^{-\lambda_i^2(tD_V/L^2)} \cos[\lambda_i z/L] \tag{11}$$

where

$$A_i = \int_0^L \cos[\lambda_i z/L]\,dz \Big/ \int_0^L \cos^2[\lambda_i z/L]\,dz \tag{12}$$

and where λ_i is the ith root of the equation $Lk_S\sigma_S/(2D_V) = \lambda_i \tan \lambda_i$. In this calculation, the form of the solution is known, but the parameter $k_S\sigma_S$ is not. Finally, the molality in the core region can be analytically averaged using the formula

$$\bar{m}(t) = l^{-1}\int_0^l m(z,t)\,dz \tag{13}$$

where l = 10 Å is the half-width of the core solution.

Equations 10−13 combined with values $D_V = 1.55 \times 10^{-9}$ m^2/s (cf., Supporting Information, section SI2.1) and L = 25 Å can be used to model the results of Aragones et al.[49] as diffusion to the slab surface followed by a surface reaction (attachment). The one unknown parameter is $k_S\sigma_S$. The analytical curve $\bar{m}(t)$ fits the data of Aragones et al.[49] well when $k_S\sigma_S$ = 0.006 m/s. The value obtained from the simulations of attachment to a flat slab is approximately 10 times smaller than $k_S\sigma_S$ values obtained from our simulations of attachment to small nuclei. This may be explained by a smaller density of attachment sites on a flat slab than on the curved (rough) nuclei. Despite the difference in $k_S\sigma_S$, both analyses clearly show that ion desolvation—not diffusion through the bulk solution—is the limiting resistance to ion attachment to nuclei as well as to flat crystal faces. The computational results also confirm an experimentally observed connection between growth rates and prefactors in nucleation kinetics.[91]

EFFECTIVE INTERFACIAL FREE ENERGY

Thus far, we have identified the driving force, the critical nucleus size, and the attachment frequency as a function of molality. All of these properties were determined directly from simulations of nuclei and bulk phases with no reference to classical nucleation theory. We have not yet determined the interfacial free energy, and we wish not to use the interfacial energy from a macroscopic flat interface. Following Knott et al.,[34] the effective interfacial free energies of small nuclei can be estimated by using eq 14 to model the initial behavior of the trajectories in Figure 4:

$$\left.\frac{d\langle n(t)\rangle}{dt}\right|_{t=0} = -\frac{D}{k_BT}\left(-\Delta\mu + \frac{2\gamma a}{3\langle n(0)\rangle^{1/3}}\right) \tag{14}$$

Because the nucleus size does not change rapidly, we estimate the initial slopes in Figure 4 from the average slope over the first 4 ns. We assume a nucleus shape factor of $a = 4.04 \times 10^{-19}$ m^2 from $4\pi(3v_0/4\pi)^{2/3}$, with v_0 being the volume per ion in the crystal structure. All errors arising from this assumption are lumped into the effective interfacial free energy, γ, which is obtained by minimizing squared residuals of $d\langle n(t)\rangle/dt$.

DOI: 10.1021/jacs.5b08098
J. Am. Chem. Soc. 2015, 137, 13352−13361

Two different procedures were employed to determine the interfacial free energy. First, we estimated a single molality-independent interfacial free energy $\gamma = 47$ mJ/m^2 by simultaneously fitting to swarms from all supersaturations. Second, we determined three separate interfacial free energies for each of the three supersaturated molalities. The resulting interfacial free energies (Table 1) range from 41 to 63 mJ/m^2.

Table 1. Interfacial Free Energies from Fitting Nucleus Drift Velocities

m (mol/kg)	γ (mJ/m^2)
–	47[a]
8	41
10	54
12	63

[a]The value is a single interfacial free energy obtained from all state points.

Analysis of variance suggests that the molality dependence is statistically significant. However, the separate γ values may be compensating for errors in the assumed shape factor, in the attachment frequency model, and in the assumption that bulk and surface energies are clearly separable, as implied by eq 3. On average, our predictions differ by a factor of 1.7 from the experimental estimate given by Na et al.[26] (87 mJ/m^2).

NUCLEATION RATES

We now have all the required quantities to estimate a nucleation rate. However, we begin with an estimate of the maximum possible nucleation rate, by assuming that every associated ion pair is a postcritical nucleus that will irreversibly grow. Hence, the typical inverse lifetime, $1/t_a$, of Na^+ and Cl^- ions, along with their density, ρ_{ions}, provides an upper bound to the nucleation rate: $J \leq \rho_{ions}/t_a$. Figure 7a shows that the free energy as a function of r_{Na-Cl} has separate minima corresponding to associated ions and solvent-separated ions. The free energy surface identifies a distance, $r^{\ddagger}_{Na-Cl} = 3.5$ Å, that separates the associated ion population from the solvent-separated ion population.

At the high concentrations of our study, the barrier between associated and solvent-separated states is too small to obtain a proper rate constant for interconversion. However, we can estimate the lifetime of the solvent-separated ions from the time-correlation function $R_a(t)$, defined by

$$R_a(t) = \frac{\langle h_{ssp}(r_{Na-Cl},0)\, h_{ap}(r_{Na-Cl},t)\rangle}{\langle h_{ssp}(r_{Na-Cl})\rangle\langle h_{ap}(r_{Na-Cl})\rangle} \quad (15)$$

where $h_{ssp} = 1$ if $r_{Na-Cl} > r^{\ddagger}_{Na-Cl}$ and 0 otherwise and $h_{ap} = 1$ if $r_{Na-Cl} < r^{\ddagger}_{Na-Cl}$ and 0 otherwise. The typical association time was slightly molality-dependent but always on the order of 0.1 ps (Figure 7b). Combining the estimated lifetime of separated ions with the ion concentration gives an upper bound to the nucleation rate as approximately 10^{35}/(cm^3 s).

The driving forces, attachment frequencies, and interfacial free energies from our simulations are used in conjunction with classical nucleation theory to estimate the nucleation rate: $J = \rho_{ions} DZ \exp[-\Delta G/(k_B T)]$. The Supporting Information outlines the separate components of the calculation: nucleation barriers ($\Delta G/k_B T$), Zeldovich factors (Z), and attachment frequencies at the critical size (D). The nucleation rates from the seeded simulations are presented in Figure 8 together with the upper bound and with rates estimated from measurements.[26,28,29] The

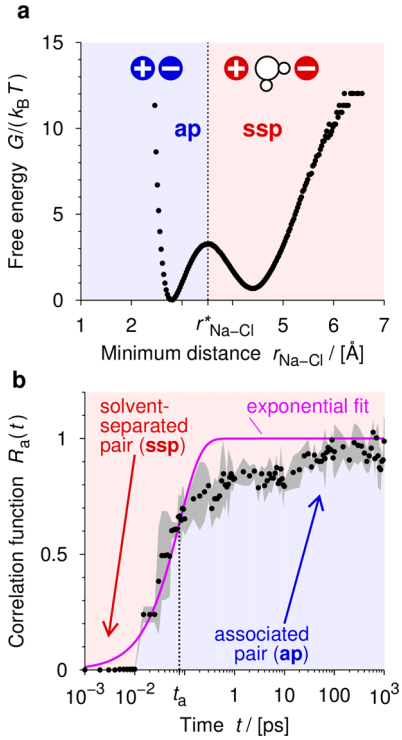

Figure 7. (a) The free-energy profile, $G(r_{Na-Cl})/(k_B T)$, along the distance between a tagged sodium ion to its nearest counterion has an associated pair (ap) minimum, a minimum for solvent-separated ions (ssp), and a barrier between the minima at $r^{\ddagger}_{Na-Cl} = 3.5$ Å. The small barrier allowed us to directly compute $P(r_{Na-Cl})$ from a simulation with no importance sampling, yielding $G/(k_B T) = -\ln P(r_{Na-Cl})$. (b) From the time correlation function, $R_a(t)$, we can identify the typical lifetime (t_a) of initially separated counterions: $t_a = 0.08$ ps at $m = 10$ mol/kg. The gray curves are error bars. The data in both parts a and b represent averages from three independent simulations.

Supporting Information also provides a description of the measurements and the determination of the driving force (section S3.1). The upper bound, the computed nucleation rates, and even the experiments converge for high driving forces when $1/[\Delta\mu/(k_B T)]^2 \to 0$. At lower driving forces, there are large discrepancies from 15 to 30 orders of magnitude.

Even for the simplest nucleation processes (e.g., crystallization from a compressed hard sphere fluid), such large disagreements between experiment and simulation are mysteriously typical.[92−94] There are several potential sources for the discrepancy in our own study. While we did not use the macroscopic interfacial free energy, we did use some potentially problematic elements of classical nucleation theory. These include the assumption that nuclei are spherical with a continuum of sizes. It is also possible that the Joung−Cheatham force field,[48] while providing a satisfactory description of bulk properties, does not yield an accurate description of interfacial properties.[95] A small increase in the interfacial free energy would dramatically reduce the computed nucleation rates, because it is cubed in the barrier to nucleation. The extent of this parameter's sensitivity is clearly seen in Figure 8. The mutual interfacial free energy from fitting the CNT rate to all three experimental data points is roughly twice our estimate of γ. The rates, however, differ by up to 30 orders of magnitude!

It should also be noted that the experiments themselves are not absolutely inculpable. Draper et al.[96] have shown that a net charge present in the levitated droplet can promote nucleation.

DOI: 10.1021/jacs.5b08098
J. Am. Chem. Soc. 2015, 137, 13352−13361

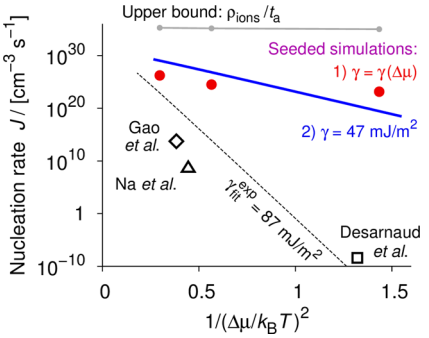

Figure 8. Comparison of our predictions of the steady-state nucleation rate, J, using atomistic simulations with estimates from experiments employing an electrodynamic levitator trap,[26] an efflorescence chamber,[28] and microcapillaries,[29] respectively, at comparable driving forces. We also include an upper bound based on ion-pair association times, t_a (cf., Figure 7), and ion concentrations, ρ_{ions}. Additionally, we fitted the interfacial free energy, γ_{fit}^{exp}, to all experimental rates by using CNT and minimizing the residuals in $\ln(J)$. This yielded a range for γ_{fit}^{exp} between 83 and 87 mJ/m^2, depending on which ρ_{ions} and a are used (simulations vs experiments). The values are very close to the interfacial free energy reported by Na et al.[26] Finally, note that the rate given by Olsen et al.[27] is not included because we could not determine the corresponding driving force. Their rate estimate is 5 orders of magnitude lower than the rate determined by Na et al.,[26] who used the same technique. However, Olsen et al.[27] probed much longer induction times ($t_{ind} \approx 1$ h, whereas Na et al.[26] reported t_{ind} on the order of 1 s). Consequently, the typical supersaturation at the moment of nucleation should have been lower in the measurements by Olsen et al.[27] Hence, the rate reported by Olsen et al.[27] should still be in line with the overall experimental trend compiled here.

However, our computed rates are *faster* than the experimental rates. Hence, the effect noted by Draper et al.[96] cannot account for our discrepancies. Langer[97] has shown that equating the nucleation time to the time at which nuclei reach observable sizes[98,99] may lead to rate estimates that are many orders of magnitude too slow. More generally, the three experimental measurements in the literature loosely follow a trend, but they do not overlap with each other at any one condition. Thus, we cannot be completely sure that these very different measurement techniques are consistent with each other. Across the solute precipitate nucleation literature, there is a tremendous need for rate measurements that systematically span different temperatures and supersaturations. Hammadi et al.[100] have recently provided a systematic analysis of NaCl nucleation from aqueous solutions. However, they observed nucleation at the interface between a droplet and a microfluidics device. Still, their microfluidics approaches provide an exciting future opportunity for synergy between experiment and theory.

Interestingly, the upper bound, the computed nucleation rates, and even the experiments converge near the limit of metastability, where $1/[\Delta\mu/(k_BT)]^2 \to 0$. The results obtained here suggest that the easily computed upper bound in combination with a single experimental nucleation rate or knowledge of the appropriate interfacial free energy might provide reasonable estimates of the nucleation rate as a function of supersaturation.

CONCLUSIONS

To investigate an earlier report of NaCl nucleation via wurtzite-like clusters, we developed local order parameters and nucleus size coordinates that distinguish wurtzite and rock salt nuclei. Because the stability of the wurtzite structure is overestimated with the GROMOS[85] force field, our study focused on rock salt nuclei modeled with the Joung−Cheatham force field for NaCl and SPC/E water. Aragones et al.[49] have shown that this force field accurately predicts the solubility and a molality-dependent chemical potential, that is, the driving force for NaCl nucleation including nonidealities.

We have used a seeded simulation approach to investigate the processes and kinetics by which NaCl nuclei form in aqueous solution. We proposed and used new criteria to ensure that growth and dissolution is not influenced by depletion. The seeded simulations allowed us to identify the critical nucleus size and the ion-attachment frequency at three different supersaturations. We also independently determined the attachment frequencies from the coexistence simulation data of Aragones et al.,[49] by using a diffusion model with reactive boundary conditions. The two approaches give attachment frequencies that are a factor of 10 from each other. However, both approaches clearly underline that attachment is limited by ion desolvation and not by diffusion to the attachment sites through the solution.

We used the seeded trajectory data to estimate the interfacial free energy between the NaCl nucleus and the brine solution as 47 mJ/m^2. The interfacial free energy, the driving forces, and the ion-attachment frequencies allowed us to calculate the nucleation rate at three different supersaturations. The computed nucleation rates are consistently faster than three experimental estimates: 10^{15} too fast at the highest experimental supersaturations and 10^{30} too fast at the lowest experimental supersaturations. We also compute an upper bound for the nucleation rate from the pairwise ion-association time. The experimental and computational data seem to approach this upper bound in the limit of high supersaturation.

Finally, we discuss assumptions in the computational procedures that may have contributed to the marked deviation of our rate prediction in comparison to the measurements from literature. We also emphasize the need for experimental solute precipitate nucleation rates that span wide and overlapping supersaturation intervals, so that different measurements can be compared to each other and to computational results.

ASSOCIATED CONTENT

Supporting Information

The Supporting Information is available free of charge on the ACS Publications website at DOI: 10.1021/jacs.5b08098.

Details on models and methods, complementary simulation results, and driving force determination associated with experimental results from literature (PDF)
Movie illustrating the seeded simulation approach (MPG)
LAMMPS routines written for and used in this work (ZIP)

AUTHOR INFORMATION

Corresponding Author

*baronp@engineering.ucsb.edu

Present Addresses

[‖]Computational Research Division, Lawrence Berkeley National Laboratory, Berkeley, CA 94720.
[⊥]School of Mathematics and Physics, University of Lincoln, Lincolnshire LN6 7TS, UK

Notes

The authors declare no competing financial interest.

DOI: 10.1021/jacs.5b08098
J. Am. Chem. Soc. 2015, 137, 13352−13361

■ ACKNOWLEDGMENTS

N.E.R.Z. and B.P. acknowledge support from NSF CAREER award no. 0955502. B.V. and D.Q. were supported by EPSRC grant EP/H00341X/1. Furthermore, we acknowledge support from the Center for Scientific Computing from the CNSI, MRL: NSF MRSEC (DMR-1121053) and NSF CNS-0960316.

■ REFERENCES

(1) Sear, R. P. *Int. Mater. Rev.* **2012**, *57*, 328.
(2) Agarwal, V.; Peters, B. In *Adv. Chem. Phys.*; John Wiley & Sons, Inc.: New York, 2014; Vol. *155*, p 97.
(3) Davey, R. J.; Schroeder, S. L. M.; ter Horst, J. H. *Angew. Chem., Int. Ed.* **2013**, *52*, 2166.
(4) Alpert, P. A.; Aller, J. Y.; Knopf, D. A. *Atmos. Chem. Phys.* **2011**, *11*, 5539.
(5) Hudait, A.; Molinero, V. *J. Am. Chem. Soc.* **2014**, *136*, 8081.
(6) Fransen, M.; Sachteleben, E.; Hruby, J.; Smeulders, D. M. J. *Exp. Fluids* **2014**, *55*, 1780.
(7) Perez, A.; Rubio, A. *J. Chem. Phys.* **2011**, *135*, 244505.
(8) Theofanous, T. G.; Tu, J. P.; Dinh, A. T.; Dinh, T. N. *Exp. Therm. Fluid Sci.* **2002**, *26*, 775.
(9) Gong, S.; Cheng, P. *Int. J. Heat Mass Transfer* **2013**, *64*, 122.
(10) Mochizuki, K.; Matsumoto, M.; Ohmine, I. *Nature* **2013**, *498*, 350.
(11) Schmeisser, M.; Iglev, H.; Laubereau, A. *J. Phys. Chem. B* **2007**, *111*, 11271.
(12) Beckham, G. T.; Peters, B.; Starbuck, C.; Variankaval, N.; Trout, B. L. *J. Am. Chem. Soc.* **2007**, *129*, 4714.
(13) Brill, T. B.; Karpowicz, R. J. *J. Phys. Chem.* **1982**, *86*, 4260.
(14) Yi, P.; Rutledge, G. C. *J. Chem. Phys.* **2009**, *131*, 134902.
(15) Vogel, J.; Kuch, W.; Bonfim, M.; Camarero, J.; Pennec, Y.; Offi, F.; Fukumoto, K.; Kirschner, J.; Fontaine, A.; Pizzini, S. *Appl. Phys. Lett.* **2003**, *82*, 2299.
(16) Radhakrishnan, R.; Trout, B. L. *J. Am. Chem. Soc.* **2003**, *125*, 7743.
(17) Slater, B.; Quigley, D. *Nat. Mater.* **2014**, *13*, 670.
(18) Sanz, E.; Vega, C.; Espinosa, J. R.; Caballero-Bernal, R.; Abascal, J. L. F.; Valeriani, C. *J. Am. Chem. Soc.* **2013**, *135*, 15008.
(19) Bullock, G.; Molinero, V. *Faraday Discuss.* **2013**, *167*, 371.
(20) Ickes, L.; Welti, A.; Hoose, C.; Lohmann, U. *Phys. Chem. Chem. Phys.* **2015**, *17*, 5514.
(21) McPherson, A.; Shlichta, P. *Science* **1988**, *239*, 385.
(22) Poon, G. G.; Seritan, S.; Peters, B. *Faraday Discuss.* **2015**, *179*, 329.
(23) Lin, Y.; Ding, F.; Yakobson, B. I. *Phys. Rev. B: Condens. Matter Mater. Phys.* **2008**, *78*, 041402.
(24) Hamm, L. M.; Giuffre, A. J.; Han, N.; Tao, J. H.; Wang, D. B.; De Yoreo, J. J.; Dove, P. M. *Proc. Natl. Acad. Sci. U. S. A.* **2014**, *111*, 1304.
(25) Duffy, D. M.; Harding, J. H. *Langmuir* **2004**, *20*, 7630.
(26) Na, H. S.; Arnold, S.; Myerson, A. S. *J. Cryst. Growth* **1994**, *139*, 104.
(27) Olsen, A. P.; Flagan, R. C.; Kornfield, J. A. *Rev. Sci. Instrum.* **2006**, *77*, 073901.
(28) Gao, Y.; Yu, L. E.; Chen, S. B. *J. Phys. Chem. A* **2007**, *111*, 10660.
(29) Desarnaud, J.; Derluyn, H.; Carmeliet, J.; Bonn, D.; Shahidzadeh, N. *J. Phys. Chem. Lett.* **2014**, *5*, 890.
(30) Chianese, A.; Dicave, S.; Mazzarotta, B. *J. Chem. Eng. Data* **1986**, *31*, 329.
(31) Kashchiev, D.; Verdoes, D.; Vanrosmalen, G. M. *J. Cryst. Growth* **1991**, *110*, 373.
(32) Peters, B. *J. Cryst. Growth* **2011**, *317*, 79.
(33) Maggioni, G. M.; Mazzotti, M. *Faraday Discuss.* **2015**, *179*, 359.
(34) Knott, B. C.; Molinero, V.; Doherty, M. F.; Peters, B. *J. Am. Chem. Soc.* **2012**, *134*, 19544.
(35) Wedekind, J.; Reguera, D.; Strey, R. *J. Chem. Phys.* **2006**, *125*, 214505.
(36) Duff, N.; Peters, B. *J. Chem. Phys.* **2009**, *131*, 184101.
(37) Agarwal, V.; Peters, B. *J. Chem. Phys.* **2014**, *140*, 084111.
(38) Adams, D. J. *Mol. Phys.* **1975**, *29*, 307.
(39) Adams, D. J. *Mol. Phys.* **1974**, *28*, 1241.
(40) Moucka, F.; Lisal, M.; Smith, W. R. *J. Phys. Chem. B* **2012**, *116*, 5468.
(41) Kusaka, I.; Wang, Z. G.; Seinfeld, J. H. *J. Chem. Phys.* **1998**, *108*, 3416.
(42) Moucka, F.; Lisal, M.; Skvor, J.; Jirsak, J.; Nezbeda, I.; Smith, W. R. *J. Phys. Chem. B* **2011**, *115*, 7849.
(43) Perego, C.; Salvalaglio, M.; Parrinello, M. *J. Chem. Phys.* **2015**, *142*, 144113.
(44) Reguera, D.; Bowles, R. K.; Djikaev, Y.; Reiss, H. *J. Chem. Phys.* **2003**, *118*, 340.
(45) Grossier, R.; Veesler, S. *Cryst. Growth Des.* **2009**, *9*, 1917.
(46) Schmelzer, J. W. P.; Abyzov, A. S. *J. Non-Cryst. Solids* **2014**, *384*, 2.
(47) Salvalaglio, M.; Perego, C.; Giberti, F.; Mazzotti, M.; Parrinello, M. *Proc. Natl. Acad. Sci. U. S. A.* **2015**, *112*, E6.
(48) Joung, I. S.; Cheatham, T. E. *J. Phys. Chem. B* **2009**, *113*, 13279.
(49) Aragones, J. L.; Sanz, E.; Vega, C. *J. Chem. Phys.* **2012**, *136*, 244508.
(50) Zahn, D. *Phys. Rev. Lett.* **2004**, *92*, 040801.
(51) Giberti, F.; Tribello, G. A.; Parrinello, M. *J. Chem. Theory Comput.* **2013**, *9*, 2526.
(52) Chakraborty, D.; Patey, G. N. *J. Phys. Chem. Lett.* **2013**, *4*, 573.
(53) Chakraborty, D.; Patey, G. N. *Chem. Phys. Lett.* **2013**, *587*, 25.
(54) Nahtigal, I. G.; Zasetsky, A. Y.; Svishchev, I. M. *J. Phys. Chem. B* **2008**, *112*, 7537.
(55) Alejandre, J.; Hansen, J. P. *Phys. Rev. E* **2007**, *76*, 061505.
(56) ten Wolde, P. R.; Frenkel, D. *Science* **1997**, *277*, 1975.
(57) Anderson, V. J.; Lekkerkerker, H. N. W. *Nature* **2002**, *416*, 811.
(58) Vekilov, P. G. *Cryst. Growth Des.* **2004**, *4*, 671.
(59) Erdemir, D.; Lee, A. Y.; Myerson, A. S. *Acc. Chem. Res.* **2009**, *42*, 621.
(60) Nielsen, M. H.; Aloni, S.; De Yoreo, J. J. *Science* **2014**, *345*, 1158.
(61) Gebauer, D.; Colfen, H. *Nano Today* **2011**, *6*, 564.
(62) Peters, B. *J. Chem. Phys.* **2011**, *135*, 044107.
(63) Auer, S.; Frenkel, D. *Annu. Rev. Phys. Chem.* **2004**, *55*, 333.
(64) Valeriani, C.; Sanz, E.; Frenkel, D. *J. Chem. Phys.* **2005**, *122*, 194501.
(65) Horsch, M.; Vrabec, J.; Hasse, H. *Phys. Rev. E* **2008**, *78*, 011603.
(66) Zykova-Timan, T.; Valeriani, C.; Sanz, E.; Frenkel, D.; Tosatti, E. *Phys. Rev. Lett.* **2008**, *100*, 036103.
(67) Berendsen, H. J. C.; Grigera, J. R.; Straatsma, T. P. *J. Phys. Chem.* **1987**, *91*, 6269.
(68) Abascal, J. L. F.; Vega, C. *J. Chem. Phys.* **2005**, *123*, 234505.
(69) Lu, J. B.; Qiu, Y. Q.; Baron, R.; Molinero, V. *J. Chem. Theory Comput.* **2014**, *10*, 4104.
(70) Fumi, F. G.; Tosi, M. P. *J. Phys. Chem. Solids* **1964**, *25*, 31.
(71) Ferrario, M.; Ciccotti, G.; Spohr, E.; Cartailler, T.; Turq, P. *J. Chem. Phys.* **2002**, *117*, 4947.
(72) Smith, D. E.; Dang, L. X. *J. Chem. Phys.* **1994**, *100*, 3757.
(73) Moucka, F.; Nezbeda, I.; Smith, W. R. *J. Chem. Theory Comput.* **2013**, *9*, 5076.
(74) Sanz, E.; Vega, C. *J. Chem. Phys.* **2007**, *126*, 014507.
(75) Hockney, R. W.; Eastwood, J. W. *Computer Simulation Using Particles*, 1st ed.; Adam Hilger: New York, 1989.
(76) Ryckaert, J. P.; Ciccotti, G.; Berendsen, H. J. C. *J. Comput. Phys.* **1977**, *23*, 327.
(77) Plimpton, S. *J. Comput. Phys.* **1995**, *117*, 1.
(78) Shinoda, W.; Shiga, M.; Mikami, M. *Phys. Rev. B: Condens. Matter Mater. Phys.* **2004**, *69*, 134103.
(79) Shetty, R.; Escobedo, F. A.; Choudhary, D.; Clancy, P. *J. Chem. Phys.* **2002**, *117*, 4000.
(80) Peters, B. *J. Chem. Phys.* **2009**, *131*, 244103.
(81) Duff, N.; Peters, B. *J. Chem. Phys.* **2011**, *135*, 134101.
(82) Santiso, E. E.; Trout, B. L. *J. Chem. Phys.* **2011**, *134*, 064109.
(83) Beckham, G. T.; Peters, B. *J. Phys. Chem. Lett.* **2011**, *2*, 1133.
(84) Jungblut, S.; Singraber, A.; Dellago, C. *Mol. Phys.* **2013**, *111*, 3527.
(85) Oostenbrink, C.; Villa, A.; Mark, A. E.; Van Gunsteren, W. F. *J. Comput. Chem.* **2004**, *25*, 1656.
(86) Auer, S.; Frenkel, D. *J. Chem. Phys.* **2004**, *120*, 3015.

DOI: 10.1021/jacs.5b08098
J. Am. Chem. Soc. 2015, 137, 13352−13361

(87) Israelachvili, J. N. *Intermolecular and Surface Forces*, 3rd ed.; Academic Press: New York, 2001.
(88) Pan, A. C.; Sezer, D.; Roux, B. *J. Phys. Chem. B* **2008**, *112*, 3432.
(89) Joswiak, M. N.; Duff, N.; Doherty, M. F.; Peters, B. *J. Phys. Chem. Lett.* **2013**, *4*, 4267.
(90) Lundrigan, S. E. M.; Saika-Voivod, I. *J. Chem. Phys.* **2009**, *131*, 104503.
(91) Davey, R. J.; Back, K. R.; Sullivan, R. A. *Faraday Discuss.* **2015**, *179*, 9.
(92) Oxtoby, D. W. *Acc. Chem. Res.* **1998**, *31*, 91.
(93) Filion, L.; Hermes, M.; Ni, R.; Dijkstra, M. *J. Chem. Phys.* **2010**, *133*, 244115.
(94) Filion, L.; Ni, R.; Frenkel, D.; Dijkstra, M. *J. Chem. Phys.* **2011**, *134*, 134901.
(95) Liu, L. M.; Laio, A.; Michaelides, A. *Phys. Chem. Chem. Phys.* **2011**, *13*, 13162.
(96) Draper, N. D.; Bakhoum, S. F.; Haddrell, A. E.; Agnes, G. R. *J. Am. Chem. Soc.* **2007**, *129*, 11364.
(97) Langer, J. S. In *Systems far from Equilibrium*; Garrido, L., Ed.; Springer-Verlag: Sitges, Spain, 1980; p 12.
(98) Binder, K.; Stauffer, D. *Adv. Phys.* **1976**, *25*, 343.
(99) Langer, J. S.; Schwartz, A. J. *Phys. Rev. A: At., Mol., Opt. Phys.* **1980**, *21*, 948.
(100) Hammadi, Z.; Grossier, R.; Zhang, S.; Ikni, A.; Candoni, N.; Morin, R.; Veesler, S. *Faraday Discuss.* **2015**, *179*, 489.

DOI: 10.1021/jacs.5b08098
J. Am. Chem. Soc. 2015, 137, 13352−13361